

A method for the sequential measurement of yttrium-90 and thorium-234 and their application to the study of rapid particle dynamics in aquatic systems

James T. Waples¹* and Kent A. Orlandini²

¹Great Lakes WATER Institute, University of Wisconsin-Milwaukee, Milwaukee, WI 53204, USA

²Environmental Research Division, Argonne National Laboratory, Argonne, IL 60439, USA

Abstract

²³⁴Th/²³⁸U activity ratios have been used for decades in marine and freshwater systems as a tracer for particle flux—where disequilibrium between particle-reactive ²³⁴Th (half-life: 24.1 d) and its conservative parent ²³⁸U measures particle removal rates on a time scale of days to weeks. A new tracer that we have developed utilizes ⁹⁰Y/⁹⁰Sr activity ratios—where disequilibrium between particle-reactive ⁹⁰Y (half-life: 64 h) and its conservative parent ⁹⁰Sr measures particle removal rates on a time scale of hours to days. When both tracers (⁹⁰Y/⁹⁰Sr and ²³⁴Th/²³⁸U) are used in tandem, net particle removal rates on both time scales are measured. Here, we present a detailed set of instructions for the sequential measurement of ⁹⁰Y and ²³⁴Th in a water sample and demonstrate how the use of these two chronometers can be applied to deconstruct sediment resuspension in Lake Michigan.

It has been forty years since Bhat et al. (1969) first demonstrated the utility of measuring ²³⁴Th disequilibrium as a tracer for particle scavenging and flux in aquatic systems. Disequilibrium between ²³⁴Th and its parent ²³⁸U clocks particle removal on a time scale of days to weeks. A shorter-lived tracer is needed, however, to measure faster processes in aquatic systems.

A novel solution has been suggested by Orlandini et al. (2003), in which the application of ⁹⁰Y/⁹⁰Sr disequilibrium as a tracer of particle flux is demonstrated. The true advantage of the ⁹⁰Y/⁹⁰Sr tracer pair is that ⁹⁰Y has a half-life of only 64 h (2.67 d)—nearly an order of magnitude shorter than its nearest particle tracer group analog (i.e., ²³⁴Th half-life = 24.1 d).

Here, we demonstrate the use of ⁹⁰Y/⁹⁰Sr disequilibrium as a short timescale tracer of particle flux in a natural aquatic system. We elaborate on the methodology for isolating and measuring ⁹⁰Y that was first presented in Orlandini et al. (2003) and include a protocol for separating both ⁹⁰Y and ²³⁴Th from the

same sample matrix. We stress the advantage of measuring both ⁹⁰Y and ²³⁴Th disequilibrium in tandem as a means of quantifying sediment resuspension in aquatic systems and provide a proof of concept using a time series of samples collected in nearshore Lake Michigan.

Materials and procedures

A flowchart showing our approach to measure both dissolved and particle-bound fractions of both ⁹⁰Y and ²³⁴Th in a water sample are presented in Fig. 1.

Sample collection and preparation

The volume of water required to measure ²³⁴Th and ⁹⁰Y on both dissolved and particle-bound fractions will depend upon a number of factors including the activity of the parent radionuclides, the particle concentration, the affinity for both ²³⁴Th and ⁹⁰Y to particles, the degree of disequilibrium between the daughters and their respective parents, and the degree of uncertainty or propagated error to which the specific application of these tracers requires. An initial estimate of the amount of water needed to measure ⁹⁰Y and ²³⁴Th may be determined by first measuring the activity of dissolved ⁹⁰Sr and ²³⁸U. In Lake Michigan, where samples for this study were collected, ⁹⁰Sr activities at the time of collection were calculated to be 759 ± 50 dpm m⁻³ (where 1 dpm = 16.7 mBq). ²³⁸U activities averaged 230 ± 20 dpm m⁻³ (Waples et al. 2003). Accordingly, we estimated that ~50 L Lake Michigan water would be sufficient to measure both dissolved and particle-bound fractions of ⁹⁰Y and ²³⁴Th.

Water samples were collected using a submersible pump and

*Corresponding author: E-mail: *jwaples@uwm.edu

Acknowledgments

We thank the captain and crew of the RV *Neeskay* for platform support; D. Szmania, K. Weckerly, and V. Klump for sampling and analytical assistance; J. Ghorai for his assistance with statistical analysis; and Kanchan Maiti and Maria Villa for their helpful comments on methodology. We especially thank Ken Buesseler and Pere Masqué for their careful critique of this manuscript. This work was supported by the National Science Foundation Grant OCE 0351824 and the University of Wisconsin-Milwaukee Great Lakes WATER Institute.

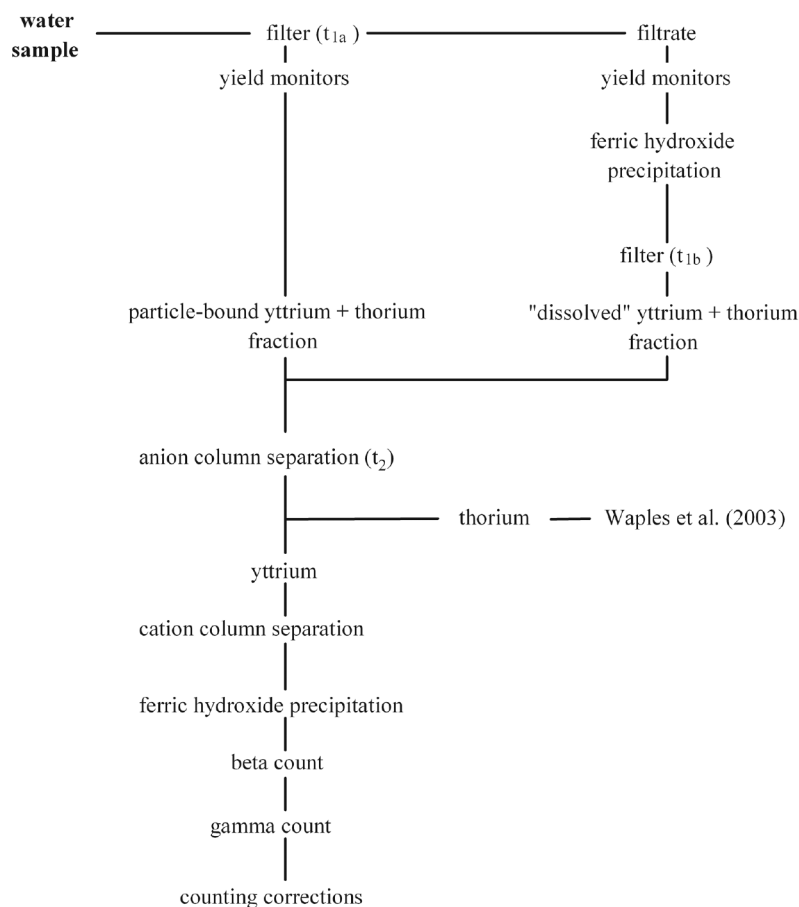


Fig. 1. A schematic for the sequential separation of ^{234}Th and ^{90}Y from a water sample.

stored briefly in 50-L plastic containers until separation of the phases by filtration. The particle-bound ($>0.45\ \mu\text{m}$) yttrium and thorium fractions were separated from the water samples by filtration through nitrocellulose filters ($0.45\ \mu\text{m}$, 293 mm, Millipore), usually within 2 h of collection. The plastic sample containers were weighed before and after filtration to determine sample volume. The time of filtration (t_{1a}) was noted, and the filter was placed in a 500-mL glass beaker. Requisite aliquot portions of the isotopic diluents, ^{88}Y (e.g., 20 dpm) and ^{229}Th (e.g., 0.5 dpm), were added to the beaker, and the sample was saved for subsequent analysis. Both yield monitors (^{88}Y and ^{229}Th) are available from Eckert & Ziegler Isotope Products.

The ($\sim 50\ \text{L}$) sample filtrate was placed in a large ($\sim 75\ \text{L}$) plastic beaker for the recovery of the dissolved yttrium and thorium fractions (operationally defined by the filter pore size). Both the yttrium and thorium were co-precipitated onto newly formed iron hydroxide with the precipitate then immediately separated by filtration. In detail, the initial filtrate was acidified with 500 mL concentrated HCl (12 M), and the requisite aliquot portions of the isotopic diluents, ^{88}Y (e.g., 20 dpm) and ^{229}Th (e.g., 0.5 dpm), were added and stirred vigorously for 15 min. Five milliliters of a strontium holdback solution ($\text{Sr}^{+2}\ 40\ \text{mg/mL}$) were added to minimize the adsorption

of strontium to the ferric hydroxide precipitate. A stock strontium holdback solution can be prepared by dissolving 97 g $\text{Sr}(\text{NO}_3)_2$ up to 1.0 L in 0.1 M HNO_3 . Next, $1\ \text{mg L}^{-1}$ ferrous iron was added (e.g., 50 mg Fe^{+2} in 50 L water) as ferrous sulfate, and the solution was again well stirred for several minutes. A stock iron solution ($\text{Fe}^{+2}\ 25\ \text{mg/mL}$) can be made by adding 10% HCl to 3.125 g $\text{FeSO}_4 \cdot 7\text{H}_2\text{O}$ up to 25 mL. Ferric hydroxide was precipitated by adding 500 mL of concentrated NH_4OH (14 M), and this precipitate was immediately collected onto a nitrocellulose filter ($0.45\ \mu\text{m}$, 293 mm, Millipore). The time of filtration (t_{1b}) was recorded, and the filter was placed in a 500-mL glass beaker and saved for subsequent analysis.

Chemical separation of yttrium and thorium

Filters carrying either the particulate or precipitated yttrium and thorium fractions were dissolved in 20 mL concentrated nitric acid (16 M) in a 500-mL glass beaker. The volume of acid used was sufficient to cover the filters. To dissolve the filters, the beakers were covered with a watch glass and heated gently for approximately 1 h or until the dark red fumes dissipated. At this time, the watch glasses were removed, and the samples were allowed to evaporate under gentle heat to dryness. Once dry, the samples were removed from heat and reconstituted with 20 mL of 8 M HNO_3 .

Separation of yttrium from thorium using ion-exchange

Yttrium was isolated from thorium by separation on an anion ion-exchange column. Disposable small columns were prepared using glass Pasteur pipettes (10.0 × 1.0 cm O.D.) and filled with anion exchange resin (Bio-Rad, AG1-X8, 100–200 mesh) to give a 6-cm column (approximately 1.0 g or ~3.5 mL of resin). The anion exchange resin column was first converted to the nitrate form using a 5-mL aliquot portion of 8 M HNO_3 . The entire sample was then transferred to the top of the column and allowed to elute before washing with an additional 20 mL of 8 M HNO_3 in four 5-mL aliquot portions. The eluate was saved for subsequent yttrium isolation.

Only thorium, plutonium, and neptunium (if present in the original sample matrix) are retained on the resin at this point (see, e.g., Saito 1984; and references therein). Thorium was separated from plutonium and eluted from the column by washing with 20 mL concentrated HCl (12 M) in four 5-mL aliquot portions. The time of elution (t_2) was noted, since ingrowth of thorium progeny began at this point. The subsequent preparation and analysis of thorium isotopes is discussed in full in Waples et al. (2003; see section 2.2.4. *Electrodeposition*).

Isolation of yttrium using ion-exchange

The yttrium fractions in 8 M HNO_3 were gently heated until dry and then reconstituted in 20 mL 1 M HCl. To isolate yttrium from other elements (particularly lead and its short-lived isotope ^{212}Pb), further separation on a cation ion-exchange column was required. Disposable small columns were prepared using glass Pasteur pipettes (10.0 × 1.0 cm O.D.) and filled with cation exchange resin (Bio-Rad, AG50W-X8, 100–200 mesh) to give a 6-cm column (approximately 1.0 g or ~3.5 mL of resin). The entire sample was then transferred to the top of the column and allowed to elute before washing with an additional ~80 mL of 1 M HCl in four 20-mL aliquot portions. Only yttrium, actinium, and the rare earth elements were retained on the resin at this point (Saito 1984; and references therein). Radium would also be retained if it was originally present in the filtered sample. However, because radium is not scavenged by the ferric hydroxide precipitate, this is not a concern. To elute the yttrium (and other rare earth-like elements), the column was washed with 30 mL of 6 M HCl in three 10-mL aliquot portions. Any thorium that may have eluted from the anion column remains strongly bound to the cation resin.

Preparing the yttrium fraction for counting

To prepare the yttrium fractions for β and γ counting, the yttrium was carried onto a second ferric hydroxide precipitation. Two mg Fe^{2+} were added to the yttrium fractions in 6 M HCl. The iron solution was prepared from a dilution of the stock iron solution described previously. Ferric hydroxide was precipitated by adding 30 mL of 7M (50% strength) NH_4OH , and this precipitate was immediately collected onto a nitrocellulose filter (0.45 μm , 47 mm, Whatman) using a Nalgene filter apparatus. While still under vacuum, the filter was rinsed three times with distilled water to remove any excess NH_4OH .

The filter was then glued (HighMark Glue Stick) to a cupped stainless steel planchet (2 inch diameter, A. F. Murphy Die & Machine Co.) and dried over gentle heat.

Yttrium sample counting

The sample planchet was first counted for beta activity using a low background gas-flow proportional counter with 2.25-in.-diameter detectors and anti-coincidence circuitry (G542 System, Gamma Products). Beta counts were measured over a minimum series of ten 250-min intervals. ^{88}Y activities were then determined by gamma spectroscopy using EG&C Ortec low background high-purity germanium (HPGe) detectors. Gamma counts were measured over an average interval of ~ 3300 min.

Beta counting strategy

To calculate the activity of ^{90}Y on particles and in the aqueous dissolved phase at the time of sample collection (i.e., t_0), estimates of the beta count rate (cpm) due specifically to ^{90}Y must first be calculated at the time of particle separation (t_{1a}) for particles and the time of the first iron precipitation (t_{1b}) for the dissolved phase. When samples containing ^{90}Y are placed within the gas-flow proportional (β) counter, beta activity from all sources is registered. If the sample is only counted once for a brief period of time (i.e., a single count method described in Waples et al. 2003), then beta counts derived from sources other than ^{90}Y (i.e., the instrument background and yield monitors) must ultimately be subtracted from the gross beta count if the true activity of ^{90}Y is to be determined.

A simple method for removing these background or non- ^{90}Y derived betas is to use a multiple count method (e.g., Aller and Cochran 1976; Buesseler et al. 2001; Waples et al. 2003). By repeatedly counting the sample over a significant fraction of the target radionuclide's life, the decline in observed activity can be used to calculate the initial activity of the target radionuclide. Specifically, repeated measurements of gross beta activity (cpm) are plotted as a function of $e^{-\lambda_y t}$, where λ_y is the decay constant for ^{90}Y (0.01083 h^{-1}) and t is the time elapsed between the beta count and the separation of ^{90}Y from its parent ^{90}Sr (i.e., t_{1a} for particles and t_{1b} for the dissolved phase). For a linear regression of the data:

$$A_{g\beta}^{cpm} = A_{b\beta}^{cpm} + A_Y^{cpm} e^{-\lambda_y t} \quad (1)$$

where $A_{g\beta}^{cpm}$ is the gross beta count and $A_{b\beta}^{cpm}$ is the total background, the initial activity of ^{90}Y (A_Y^{cpm} at t_{1a} for particles or t_{1b} for the dissolved phase) is simply the slope of the regression line, where all activities are expressed in counts per minute (cpm). The uncertainty of the estimate ($\sigma_{A_Y^{cpm}}$) is equal to the standard error of the regression.

Calculating ^{90}Y activities

The ^{90}Y activity of the sample (A_Y) in disintegrations per minute (dpm) per unit volume is finally calculated as:

$$A_Y = \frac{A_Y^{cpm}}{\text{eff} \times \text{yield} \times \text{vol}} \quad (2)$$

where *eff* is the beta detector efficiency for ^{90}Y (e.g., 0.50 cpm/dpm), *yield* is the fraction of yttrium recovered as determined by the ^{88}Y yield monitor, and *vol* is the initial sample volume (e.g., 50 L).

A small correction for ^{90}Y ingrowth in the dissolved phase sample between particle filtration (t_{1a}) and the initial iron precipitation step (t_{1b}) can be calculated as:

$$A_{Y(t_{1a})} = e^{\lambda_Y \Delta t_{1b-a}} \left(\frac{\lambda_Y A_{Sr} (e^{-\lambda_Y \Delta t_{1b-a}} - e^{-\lambda_{Sr} \Delta t_{1b-a}})}{\lambda_Y - \lambda_{Sr}} + A_{Y(t_{1b})} \right) \quad (3)$$

where λ_Y and λ_{Sr} are the decay coefficients for both radionuclides (i.e., 0.01083 h^{-1} and $2.776 \times 10^{-6} \text{ h}^{-1}$, respectively), and Δt_{1b-a} represents the amount of time elapsed between the particle filtration and the iron precipitation filtration steps. Because particles are immediately separated from the bulk sample, corrections for ^{90}Y ingrowth between sample collection (t_0) and particle filtration (t_{1a}) are assumed to be negligible (i.e., $A_{t_{1a}} \approx A_{t_0}$).

Detector efficiencies

To calculate the activity of ^{90}Y , the detector efficiency or beta cpm/dpm ratio of ^{90}Y (*eff*) is required as is the gamma cpm/dpm ratio of our yield monitor, ^{88}Y (eff_{88}). In addition, both yield monitors used here (i.e., ^{88}Y for ^{90}Y and ^{229}Th for ^{234}Th) also have the potential to bias the ^{90}Y beta count.

^{90}Y beta efficiency—To measure the gas-flow proportional (β) counter efficiency for ^{90}Y , measured aliquots of a 18.5 ± 0.1 dpm mL^{-1} ^{90}Sr standard solution prepared on 15 July 2004 (^{90}Sr half-life = 28.78 y, Argonne National Laboratory, also available from Eckert & Ziegler Isotope Products) in secular equilibrium with its daughter (^{90}Y) were added to 20 mL of 10% HCl. To this solution, 50 μL of the Sr^{2+} holdback carrier solution and 1 mL of the 2 mg $\text{Fe}^{+2} \text{ mL}^{-1}$ ($\text{FeSO}_4 \cdot 7\text{H}_2\text{O}$) solution (described above) were also added. The solution was then made basic by slowly adding concentrated NH_4OH (several milliliters) and the resulting precipitate was then filtered and prepared for counting as described in the “preparing the yttrium fraction for counting” section above. To assure quantitative scavenging, the resulting filtrate was re-acidified with concentrated HCl to which 1 mL of the 2 mg $\text{Fe}^{+2} \text{ mL}^{-1}$ solution and concentrated NH_4OH were again added. This precipitate was then again filtered and prepared for counting whereupon both sample plates (i.e., plate A containing the initial precipitate and plate B containing the second precipitate) were immediately placed into the gas-flow proportional (β) detector and counted over a series of ~ fifteen 60-min intervals. The repeated measurements of gross beta activity (cpm) were then plotted as a function of $e^{-\lambda_Y t}$ to determine A_Y^{cpm} for both plates as in Eq. 1.

The true activity of ^{90}Y (in cpm) is first corrected for the efficiency of extraction by:

$$A_Y^{cpm} = \frac{{}^A A_Y^{cpm}}{1 - \frac{{}^B A_Y^{cpm}}{{}^A A_Y^{cpm}}} \quad (4)$$

where ${}^A A_Y^{cpm}$ and ${}^B A_Y^{cpm}$ represent the activities of plates A and B, respectively. The beta detector efficiency for ^{90}Y (*eff*) is then

simply calculated as the ratio of A_Y^{cpm} over the activity of the ^{90}Y standard solution (${}^{STD} A_Y$).

^{88}Y gamma efficiency—Standards were prepared using measured aliquots of a 43.4 ± 0.4 dpm mL^{-1} ^{88}Y standard solution prepared on 8 Oct 2007 (^{88}Y half-life = 106.6 d, Eckert & Ziegler Isotope Products cat. no. 7088, NIST traceable, total uncertainty $\pm 3.1\%$ at 99% confidence level). To measure the gamma detector efficiency for ^{88}Y , a measured volume of ^{88}Y standard solution was directly deposited onto a nitrocellulose filter (0.45 μm , 47 mm, Whatman) that had been glued to a cupped stainless steel planchet. This planchet was then placed into one of three available HPGe detectors. Counts in the known region of interest in the γ -spectrum for ^{88}Y (898 keV) were measured to determine the detector response. The 898 keV region is preferred over the 1836 keV region as it provides both the largest and sharpest peak response with very low background ($\leq 3 \times 10^{-6}$ cps). Gamma counts were measured over an average interval of ~ 1500 to ~ 6000 min. Gross gamma activity (A_{gy}^{cpm}) in the 898 keV region was first corrected for background (A_{by}^{cpm}) and then corrected for decay during counting (d_c) and decay that occurred between the standard preparation on 8 October and the start of the gamma count (d_M), where the decay corrected gamma count of ^{88}Y (A_{88}^{cpm}) is expressed as:

$$A_{88}^{cpm} = (A_{gy}^{cpm} - A_{by}^{cpm}) \times d_c \div d_M \quad (5)$$

the decay of ^{88}Y during counting (d_c) is expressed as:

$$d_c = \frac{\lambda_{88} \times t_{count}}{1 - e^{-\lambda_{88} t_{count}}} \quad (6)$$

and the decay of ^{88}Y between standard preparation and the start of the gamma count (d_M) is expressed as:

$$d_M = e^{-\lambda_{88} \Delta t} \quad (7)$$

where λ_{88} is the decay coefficient for ^{88}Y ($\lambda_{88} = 0.0065 \text{ d}^{-1}$), t_{count} is the length of time the sample was counted, and Δt is the time interval between standard preparation and the start of the gamma count.

The gamma detector efficiency for ^{88}Y (eff_{88}) is finally expressed as:

$$eff_{88} = \frac{A_{88}^{cpm}}{{}^{STD} A_{88}} \quad (8)$$

where ${}^{STD} A_{88}$ is equal to the initial activity of the ^{88}Y standard and eff_{88} is expressed in units of cpm/dpm.

^{229}Th and ^{88}Y beta efficiencies—To determine what effect the yield monitors had on beta production in the low background gas-flow proportional counter, cpm/dpm ratios were measured for both ^{88}Y and ^{229}Th samples. Four ^{88}Y samples containing 0.0, 1.0, 2.0, and 3.0 mL of a 23.6 ± 0.2 dpm mL^{-1} ^{88}Y stock standard were prepared as described in the ^{88}Y gamma efficiency section above and immediately placed into the gas-

flow proportional (β) detector. Four ^{229}Th samples containing 0.0, 0.5, 1.0, and 5.0 mL of a 1.10 ± 0.01 dpm mL^{-1} ^{229}Th stock standard solution (^{229}Th half-life = 7340 y, Eckert & Ziegler Isotope Products cat. no. 7229, NIST traceable, $\pm 3.0\%$ at 99% confidence level) were run through the entire yttrium separation procedure (i.e., anion column, cation column, and iron precipitation separations), prepared for counting on a nitrocellulose filter and cupped stainless steel planchet and immediately placed into the gas-flow proportional (β) detector. By plotting measured beta counts against known sample activities, the beta cpm/dpm detector efficiencies for both ^{88}Y and ^{229}Th were simply calculated as the slope of their respective linear regression lines.

Measuring ^{90}Sr

^{90}Sr was measured by way of ^{90}Y . A separate ~ 50 L water sample was first filtered (0.45 μm , 293 mm, Millipore) and then acidified with 500 mL of concentrated HCl (12 M). This solution was then allowed to sit at least two weeks to allow ^{90}Y to grow into secular equilibrium with its parent ^{90}Sr (for $^{90}\text{Y}/^{90}\text{Sr} = 0$ at t_0 , $^{90}\text{Y}/^{90}\text{Sr} = 0.973$ after 14 d). After the required incubation, the sample was then processed for ^{90}Y as described above.

Assessment

Detector efficiencies

^{90}Y beta efficiency—A total of four sets of ^{90}Y standard plates (each consisting of a plate A containing the initial Fe precipitate and plate B containing the second Fe precipitate) were prepared with 1.0 mL of the ^{90}Sr standard solution according to the method described in the “Materials and Procedures” section above. The standard was decay corrected to the time of yttrium separation to yield a ^{90}Y standard of 16.1 ± 0.1 dpm mL^{-1} . The four sets of plates were rotated through all eight of our beta detectors over a series of \sim fifteen 60-minute counting intervals in each detector (Fig. 2a). Extraction efficiencies (from Eq. 4) for all four standard sets averaged $97 \pm 2\%$. Measurements of ^{90}Y counting efficiencies (eff) in all eight detectors ranged between 0.495 and 0.534, with propagated relative errors averaging $\pm 6\%$.

^{88}Y gamma efficiency—Two standard plates were prepared with 1.0 mL of the ^{88}Y standard solution according to the method described in the “Materials and Procedures” section above. The two plates were rotated through all three of our gamma detectors over a series of at least five counting intervals in each detector. Detector efficiencies for the 898 keV peak (eff_{88}) averaged 0.0244 ± 0.0007 , 0.0150 ± 0.0005 , and 0.0189 ± 0.0005 for detectors 1, 2, and 3, respectively. The relative uncertainty in eff_{88} for all three detectors averaged $\pm 3\%$.

^{229}Th and ^{88}Y beta efficiencies— ^{229}Th decays through a long series of short-lived radionuclides: ^{229}Th , ^{225}Ra , ^{225}Ac , ^{221}Fr , ^{217}At , ^{213}Bi , ^{213}Po , ^{209}Pb , ^{209}Bi (stable). Three of these progeny nuclides (i.e., ^{225}Ra , ^{213}Bi and ^{209}Pb) decay through beta production. While the ^{229}Th itself is separated from yttrium on the anion column, and the ^{229}Th daughter, ^{225}Ra , is separated from yttrium during the second iron precipitation, the ^{229}Th

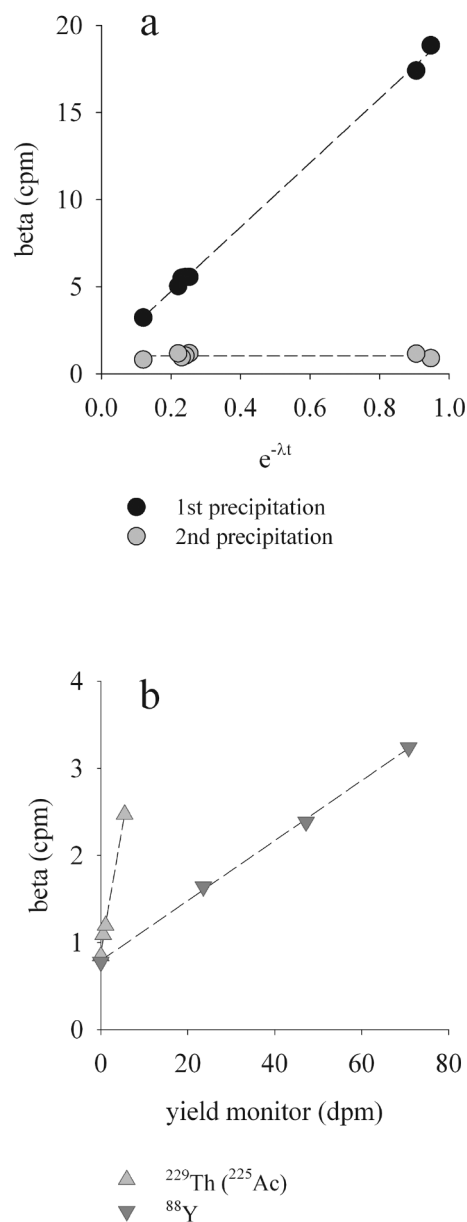


Fig. 2. (a) β decay of known ^{90}Y activity for determination of detector efficiency. (b) β detector efficiencies (cpm/dpm) for yield monitors ^{229}Th and ^{88}Y .

granddaughter, ^{225}Ac , is a rare earth element with similar behavior to yttrium. It is, therefore, effectively carried along with yttrium into the final sample matrix. Assuming 100% extraction efficiency from the ^{229}Th grandparent, the four sample plates containing 0.00, 0.55, 1.10, and 5.50 dpm ^{225}Ac were simultaneously placed in separate gas-flow proportional (β) detectors immediately after preparation and counted for one 250-min interval (Fig. 2b). The beta cpm/dpm detector efficiency for ^{225}Ac and its beta emitting daughters was calculated as the slope of linear regression through all four points to give 0.290 ± 0.010 cpm/dpm.

^{88}Y has a half-life of 106.6 d and decays to stable ^{88}Sr via electron capture (and to a much lesser extent, positron emission). Though it does not directly produce betas, the decay of ^{88}Y affects the gross beta count most likely through a combination of photoelectric effect, Compton scattering, and pair production (e.g., Friedlander et al. 1964). The four sample plates containing 0.0, 23.6, 47.2, and 70.8 dpm ^{88}Y were simultaneously placed in separate gas-flow proportional (β) detectors immediately after preparation and counted for one 250-min interval (Fig. 2b). The beta cpm/dpm detector efficiency for ^{88}Y was similarly calculated as the slope of linear regression through all four points to give 0.0345 ± 0.0007 cpm/dpm.

Beta counting strategy

A Lake Michigan water sample was filtered to remove all particles ($>0.45 \mu\text{m}$), spiked with 1.0 mL of a 1.10 ± 0.01 dpm mL^{-1} ^{229}Th standard solution and 1.0 mL of a ^{88}Y standard solution (43.4 ± 0.4 dpm mL^{-1} on 8 Oct 2007) and processed according to the yttrium separation procedures described above. Beta counting began 2.27 d after the dissolved yttrium fraction was removed from the water sample by iron precipitation (i.e., at time t_{1b}).

Short multiple count method—Estimates of the beta count rate due specifically to ^{90}Y (A_Y^{cpm}) at the time of the first iron precipitation for the dissolved phase (t_{1b}) were then calculated using the first ten (250-min) counting intervals spanning 37 h (Fig. 3a).

Gross beta counts ($A_{g\beta}^{cpm}$) were plotted as a function of $e^{-\lambda_Y t}$, where λ_Y is the decay constant for ^{90}Y (0.01083 h^{-1}) and t is the time elapsed between each beta count and the separation of ^{90}Y from its parent ^{90}Sr (i.e., t_{1b}). The initial activity of ^{90}Y at t_{1b} – equal to the slope of the regression line (A_Y^{cpm} in Eq. 1) – measured 14.70 ± 1.30 cpm, where the standard deviation of the measurement was taken as the standard error of the slope estimate. The background measured 2.26 ± 0.60 cpm ($A_{g\beta}^{cpm}$ in Eq. 1) and combined instrument background and beta contributions derived from (^{229}Th derived) ^{225}Ac progeny and ^{88}Y .

Long multiple count method—The short multiple count method is valid so long as the activity of other radionuclides that might be present in the sample matrix (and their ability to produce betas either through direct beta emission or through secondary beta production (e.g., photoelectric effects) remains constant or nearly so over the timescale of the target radionuclide's decay. Because most other elements are removed from the sample matrix during the preparation procedure, the ability for unknown environmental radionuclides to affect the calculation of a target radionuclide activity using the multiple count method is minimized. However, radionuclides purposely added to the sample matrix as yield monitors have the ability to interfere with the calculation of a target radionuclide's activity simply because yield monitors are ideally isotopes of the same target element. The production of betas by ^{88}Y and ^{225}Ac daughters is of interest only because the half-lives of these radionuclides are relevant to the timescale of ^{90}Y decay. Over the span of 5 half-lives of ^{90}Y decay (i.e.,

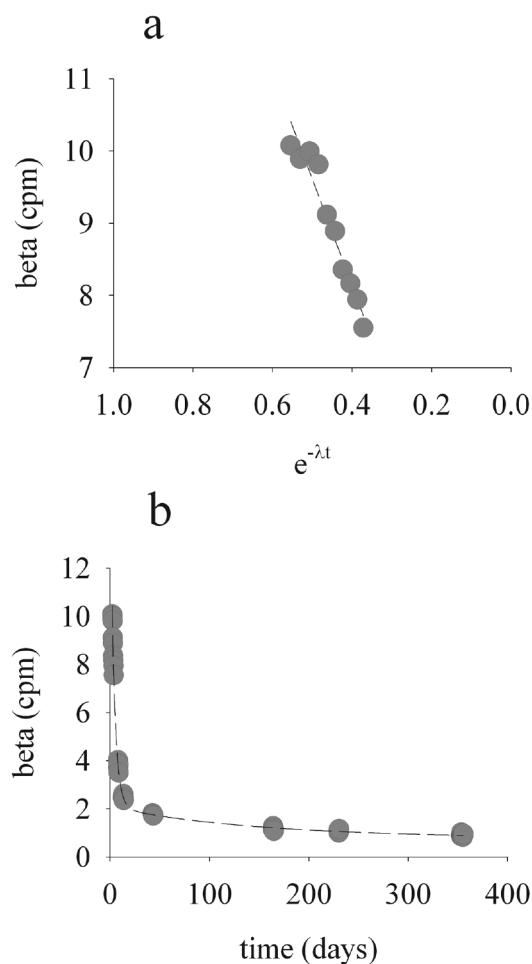


Fig. 3. (a) Short multiple β count for determining ^{90}Y activity. (b) Long multiple β count for determining ^{90}Y activity.

13.4 d), ^{88}Y decays by 8.3 % and ^{225}Ac (and its beta producing progeny) decays by 60.5 %. If betas produced by the decay of ^{88}Y and ^{225}Ac decrease significantly over the timeframe of the ^{90}Y counting interval (due to the decay of ^{88}Y and ^{225}Ac), then the estimate of ^{90}Y – as determined by the multiple count method – will be overestimated. This is an obvious concern if either the activity of yield monitors added is very high or the sample activity of ^{90}Y is very low. In the example we provide here, however, the influence of ^{88}Y and ^{225}Ac on the calculated activity of ^{90}Y is negligible. We can demonstrate this using the multiple count method over an extended period of time.

The same sample plate was counted forty more times over the course of 355 d (Fig. 3b). Repeated measurements of gross beta activity ($A_{g\beta}^{cpm}$) from all fifty (250-min) counting intervals were then plotted as a function of the time elapsed (t , days) between the beta count and the separation of ^{90}Y from its parent ^{90}Sr and fitted to a 7 parameter, triple exponential decay curve (SigmaPlot v.11, Systat Software):

$$A_{g\beta}^{cpm} = A_{b\beta}^{cpm} + A_Y^{cpm} e^{-\lambda_Y t} + A_{225}^{cpm} e^{-\lambda_{225} t} + A_{88}^{cpm} e^{-\lambda_{88} t} \quad (9)$$

where λ_Y , λ_{225} , and λ_{88} are equal to the decay coefficients of ^{90}Y , ^{225}Ac , and ^{88}Y , respectively (i.e., 0.2596 d^{-1} , 0.0693 d^{-1} and 0.0065 d^{-1}), $A_{b\beta}^{cpm}$ is equal to the instrument background (and any other steady beta activity caused by long-lived radionuclides), and A_Y^{cpm} , A_{225}^{cpm} , and A_{88}^{cpm} are equal to the activity (cpm) of ^{90}Y , ^{225}Ac , and ^{88}Y at tI , respectively.

The initial activity of ^{90}Y at tIb (A_Y^{cpm} in Eq. 9) measured $14.8 \pm 0.3\text{ cpm}$, where the standard deviation of the measurement was taken as the standard error of the estimate. This compares well with the short multiple count estimate of $14.7 \pm 1.3\text{ cpm}$ calculated above. The instrument background measured $0.77 \pm 0.03\text{ cpm}$ ($A_{b\beta}^{cpm}$ in Eq. 9) and beta contributions derived from ^{225}Ac (A_{225}^{cpm} in Eq. 9) and ^{88}Y (A_{88}^{cpm} in Eq. 9) measured 0.2 ± 0.2 and 1.29 ± 0.10 at tIb , respectively. The total background using the long multiple count method (i.e., $A_{b\beta}^{cpm} + A_{225}^{cpm} + A_{88}^{cpm}$) measured 2.3 ± 0.2 and compared well with the short multiple count method background of 2.3 ± 0.6 .

While it is true that a long count can separate beta contributions from different radionuclides (assuming these radionuclides have significantly different half-lives), the length of time required to do so here is generally prohibitive (i.e., 1.7 d for the short multiple count versus 355 d for the long multiple count). There is another advantage, however, to the long multiple count method. In a laboratory with no gamma counting facilities, the beta contributions derived from ^{88}Y (A_{88}^{cpm} in Eq. 9) can be used to determine yield. The ratio of beta contributions from ^{88}Y ($1.29 \pm 0.10\text{ cpm}$) to the measured beta detector efficiency for ^{88}Y ($0.0345 \pm 0.0007\text{ cpm/dpm}$) divided by the activity of ^{88}Y added to the sample (corrected for decay to t_1 , i.e., 39.34 dpm) gives a yield of 0.95 ± 0.07 . The average ^{88}Y yield for this particular sample, as measured on three separate gamma detectors, was equal to 0.92 ± 0.01 . A reduction in the uncertainty of the beta derived estimate of ^{88}Y yield could certainly be achieved with optimized tracer activities and counting design.

Field application

Sample collection—To demonstrate the utility of these dual tracers in the field, water samples (~50 L) were collected five times (8, 12, 16, 19 and 23 Oct 2007) at a shallow (20 meter) site in southern Lake Michigan (Fig. 4; ‘Green Can’ station; Lat: $42^\circ 59.1600\text{ N}$ Long: $87^\circ 47.9284\text{ W}$). Samples for total suspended matter and radionuclide measurements were collected from 3 m, 10 m, and 17 m depths using a submersible pump.

Ancillary data—An instrumented (PIONEER) mooring was deployed at the Green Can sampling site over the duration of the sampling period. Temperatures were recorded with thermistors at 1 m intervals and a sonde (YSI) located ~1 m above the bottom recorded turbidity, chlorophyll, and other standard parameters. All data were transmitted to our laboratory in real-time via 900 MHz radio (Consi et al. 2007). Water currents (3-D) were measured for the duration of the experiment with a bottom mounted (upward-looking) SonTek ADP (1000 kHz; averaging interval: 60 s, profiling interval: 600 s).

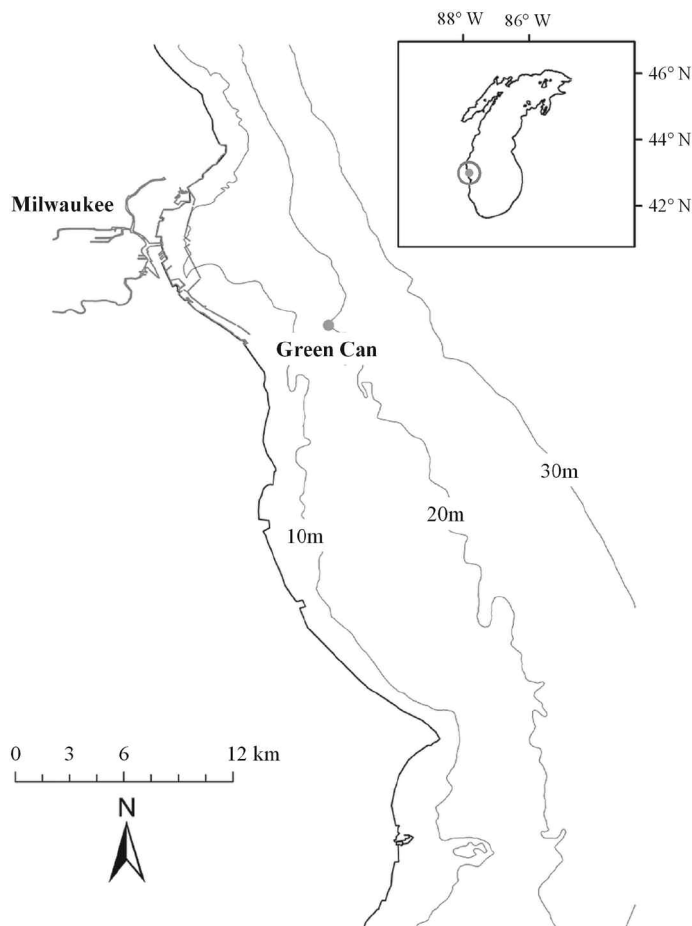


Fig. 4. ‘Green Can’ sampling station in southwestern Lake Michigan.

Results—For each large volume water sample, activities of ^{90}Y and ^{234}Th on both dissolved (diss, $<0.45\ \mu\text{m}$) and particle-bound (part, $>0.45\ \mu\text{m}$) fractions were measured (Table 1). Sample preparation (filtering to sample plate) generally took ~14 h. ^{229}Th recovery averaged 53%. ^{88}Y recovery averaged 94%. Radionuclide activity measurements from 8 Oct are omitted as ^{90}Y samples were lost during column separation. Total ^{234}Th activities ranged from a maximum of $242 \pm 4\text{ dpm m}^{-3}$ (~105% equilibrium with ^{238}U) at 17 m on 12 Oct to a minimum of $77 \pm 2\text{ dpm m}^{-3}$ (~31% equilibrium with ^{238}U) at 17 m on 23 Oct. Total ^{90}Y activities ranged from a maximum of $632 \pm 26\text{ dpm m}^{-3}$ (~83% equilibrium with ^{90}Sr) at 10 m on 16 Oct to a minimum of $449 \pm 40\text{ dpm m}^{-3}$ (~59% equilibrium with ^{90}Sr) at 17 m on 23 Oct. Average Lake Michigan ^{238}U activities of $230 \pm 20\text{ dpm m}^{-3}$ (Waples et al. 2003, 2004) and ^{90}Sr activities of $759 \pm 50\text{ dpm m}^{-3}$ (Fig. 5) were used to calculate the extent of disequilibrium between parent and daughter nuclides.

Radionuclide and particle flux—In a one-box model (see Savoye et al. 2006), the temporal change in ^{234}Th activity ($\partial A_{Th}/\partial t$) is expressed as:

$$\frac{\partial A_{Th}}{\partial t} = \lambda_{Th}(A_U - A_{Th}) - P_{Th} + V_{Th} \quad (10)$$

Table 1. Nearshore ²³⁴Th and ⁹⁰Y measurements at station ‘Green Can’ in southern Lake Michigan.

Collected	DOY	Depth (m)	TSM (g m ⁻³)	²³⁴ Th _{part} (dpm m ⁻³)	²³⁴ Th _{diss} (dpm m ⁻³)	⁹⁰ Y _{part} (dpm m ⁻³)	⁹⁰ Y _{diss} (dpm m ⁻³)
8 Oct 2007	281	3	0.3				
		10	0.5				
		17	0.2				
12 Oct 2007	285	3	3.7	123 ± 2	118 ± 3	133 ± 8	350 ± 28
		10	3.3	141 ± 2	99 ± 2	114 ± 22	336 ± 24
		17	3.9	136 ± 2	106 ± 3	117 ± 20	393 ± 20
16 Oct 2007	289	3	0.7	97 ± 3	102 ± 3	30 ± 13	585 ± 42
		10	0.7	93 ± 2	121 ± 3	69 ± 10	563 ± 24
		17	0.6	109 ± 3	101 ± 2	22 ± 9	556 ± 28
19 Oct 2007	292	3	1.0	42 ± 2	82 ± 3	7 ± 40	497 ± 15
		10	1.0	97 ± 3	88 ± 3	43 ± 19	432 ± 9
		17	1.2	56 ± 2	78 ± 2	33 ± 26	490 ± 45
23 Oct 2007	296	3	0.5	48 ± 1	47 ± 2	26 ± 21	520 ± 46
		10	0.4	47 ± 1	50 ± 2	31 ± 6	437 ± 34
		17	0.9	39 ± 1	38 ± 1	32 ± 27	417 ± 29

where the total activities of ²³⁸U (A_U) and ²³⁴Th (A_{Th}) integrated over the depth of the water column are expressed in dpm m⁻², the decay constant for ²³⁴Th (λ_{Th}) is equal to 0.02876 d⁻¹, the net downward removal flux of ²³⁴Th (P_{Th}) is expressed in dpm m⁻² d⁻¹, and V_{Th} is equal to the sum of horizontal advective and diffusive fluxes of ²³⁴Th.

Similarly, the temporal change in ⁹⁰Y activity ($\partial A_Y / \partial t$) is expressed as:

$$\frac{\partial A_Y}{\partial t} = \lambda_Y (A_{Sr} - A_Y) - P_Y + V_Y \quad (11)$$

where the total depth integrated activities of ⁹⁰Sr (A_{Sr}) and ⁹⁰Y (A_Y) are expressed in dpm m⁻², the decay constant for ⁹⁰Y (λ_Y) is equal to 0.25993 d⁻¹, the net downward removal flux of ⁹⁰Y (P_Y) is expressed in dpm m⁻² d⁻¹, and V_Y is equal to the sum of horizontal advective and diffusive fluxes of ⁹⁰Y.

Under steady-state conditions, which we will initially assume for the sake of clarity, the change in inventories of total ²³⁴Th and ⁹⁰Y remains constant over time, such that $\partial A_{Th} / \partial t$ and $\partial A_Y / \partial t$ are equal to zero. If we also assume that the sum of horizontal advective and diffusive fluxes (V_{Th} and V_Y) is negligible, then the net downward flux of ²³⁴Th (P_{Th}) and ⁹⁰Y (P_Y) can be expressed as:

$$P_{Th} = \lambda_{Th} (A_U - A_{Th}) \quad (12)$$

and

$$P_Y = \lambda_Y (A_{Sr} - A_Y) \quad (13)$$

If the ratio of mass to ²³⁴Th and ⁹⁰Y activity on particles is known (i.e., $mass / A_{Th}^p$ and $mass / A_Y^p$; expressed as g dpm⁻¹), then the downward flux of mass can be expressed using both

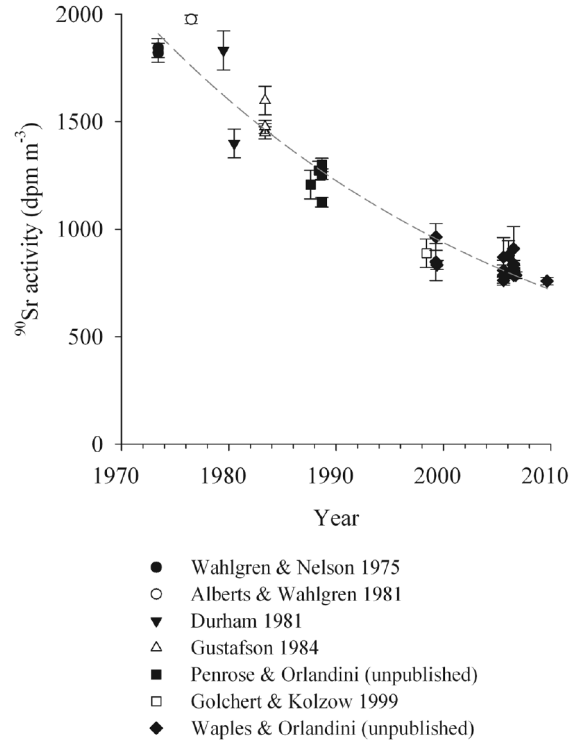


Fig. 5. ⁹⁰Sr activities in Lake Michigan over a 40 y period.

the ²³⁴Th and ⁹⁰Y tracer as:

$$P_{mass(Th)} = P_{Th} \times \frac{mass}{A_{Th}^p} \quad (14)$$

and

$$P_{mass(Y)} = P_Y \times \frac{mass}{A_Y^p} \quad (15)$$

where $P_{\text{mass}(\text{Th})}$ and $P_{\text{mass}(\text{Y})}$ are expressions of net mass flux relative to each radionuclide tracer.

The net downward flux of both ^{234}Th (P_{Th}) and ^{90}Y (P_{Y}) were calculated for four sampling days (beginning on 12 Oct) using the integrated (trapezoidal) 0-20 meter inventories of total ^{234}Th and total ^{90}Y (presented in Table 1) and Eqs. 12 and 13. The water column was isothermal (or nearly so) over the duration of the sampling period and radionuclide activities at 0 and 20 meters depth were assumed to equal those measured at 3 and 17 meters depth, respectively. The error associated with parent activities of ^{238}U and ^{90}Sr was ignored. Net mass fluxes from the water column as determined by ^{234}Th ($P_{\text{mass}(\text{Th})}$) and ^{90}Y ($P_{\text{mass}(\text{Y})}$) were calculated as the product of mass/radionuclide ratios at depth (17 m) and P_{Th} and P_{Y} , using Eqs. 14 and 15.

^{234}Th fluxes (P_{Th}) ranged from essentially zero (-6 ± 2 dpm $\text{m}^{-2} \text{d}^{-1}$) during a large resuspension event on day 285 (Fig. 6a, b) to 81 ± 1 dpm $\text{m}^{-2} \text{d}^{-1}$ at the end of the experiment on day 296 and translated to calculated mass fluxes ($P_{\text{mass}(\text{Th})}$) of essentially zero (-0.18 ± 0.06 g $\text{m}^{-2} \text{d}^{-1}$) to 1.86 ± 0.06 g $\text{m}^{-2} \text{d}^{-1}$, respectively. ^{90}Y fluxes (P_{Y}), on the other hand, measured over an order of magnitude higher at 1459 ± 155 dpm $\text{m}^{-2} \text{d}^{-1}$ on day 285 and 1423 ± 216 dpm $\text{m}^{-2} \text{d}^{-1}$ on day 296 (Fig. 6c). Resultant mass fluxes ($P_{\text{mass}(\text{Y})}$) measured 49 ± 10 g $\text{m}^{-2} \text{d}^{-1}$ and 40 ± 34 g $\text{m}^{-2} \text{d}^{-1}$, respectively. The difference in net radionuclide fluxes cannot be explained by the difference in affinity that ^{234}Th and ^{90}Y have for particulate matter. Indeed, the average distribution coefficients (K_d) for ^{234}Th and ^{90}Y (based on measurements shown in Table 1) are 1.1×10^6 and 9.4×10^4 , respectively.

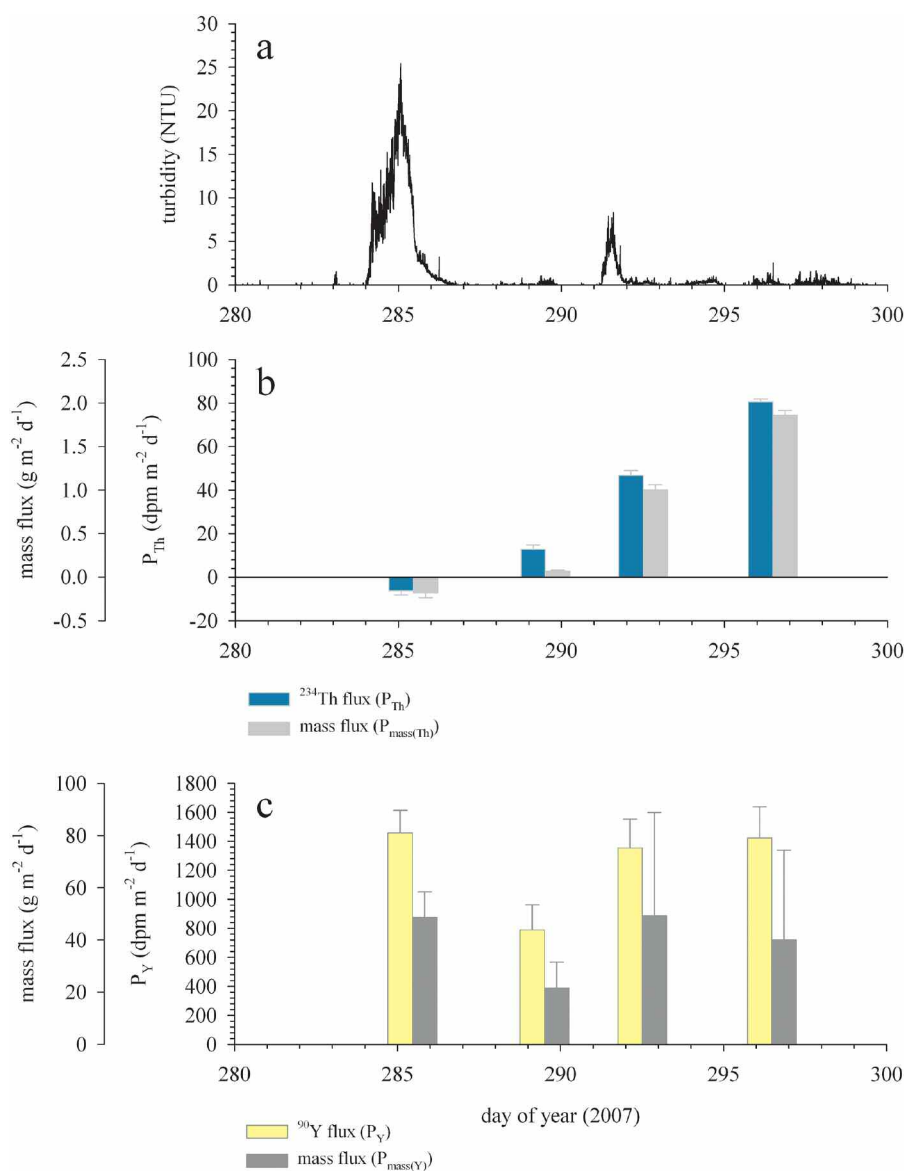


Fig. 6. (a) Turbidity at 19 m depth. (b) Steady-state ^{234}Th fluxes and mass fluxes as measured by ^{234}Th . (c) Steady-state ^{90}Y fluxes and mass fluxes as measured by ^{90}Y . Note difference in scale.

The discrepancy in radionuclide and mass fluxes can partly be explained by our assumption of steady-state conditions. If we examine the inventory of total ²³⁴Th activity over the time course of the experiment (Fig. 7), the change in ²³⁴Th activity over time ($\partial A_{Th}/\partial t$) is equal to -283 ± 31 dpm m⁻² d⁻¹ and our assumption of steady-state in Eqs. 1 and 3 is invalid. In fact, the observed decrease in ²³⁴Th activity predicts the complete removal of ²³⁴Th from the water column by day 302. The inventory of ⁹⁰Y activity, however, remains fairly constant ($\partial A_Y/\partial t = -39 \pm 182$ dpm m⁻² d⁻¹) and steady-state conditions appear reasonable.

To correct for non-steady-state conditions, the net downward flux of ²³⁴Th (P_{Th}) in Eq. 3 can be rewritten to incorporate the observed change in ²³⁴Th activity where:

$$P_{Th} = \lambda_{Th}(A_U - A_{Th}) - \frac{\partial A_{Th}}{\partial t} \quad (16)$$

By recalculating both P_{Th} and $P_{mass(Th)}$ using observed non-steady-state conditions and comparing them to P_Y and $P_{mass(Y)}$ (Fig. 8a, b), the estimates of mass flux ($P_{mass(Th)}$ and $P_{mass(Y)}$) are now more or less proportional to one another. However, the ²³⁴Th derived mass fluxes are still a factor of five to ten times lower than the ⁹⁰Y derived equivalents.

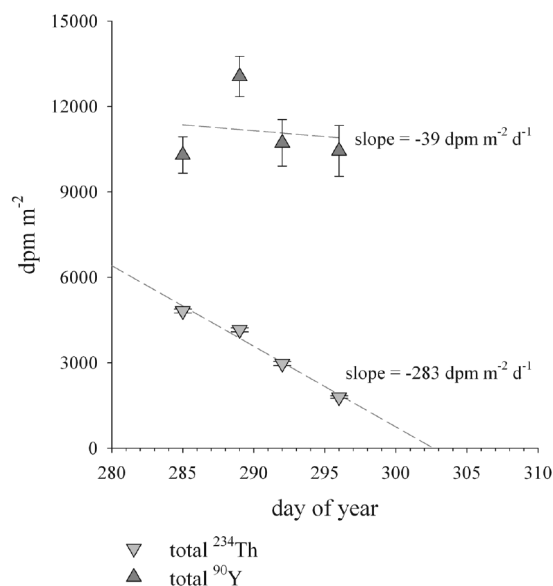


Fig. 7. Total activity of ²³⁴Th and ⁹⁰Y in 20 meter water column at 'Green Can' station.

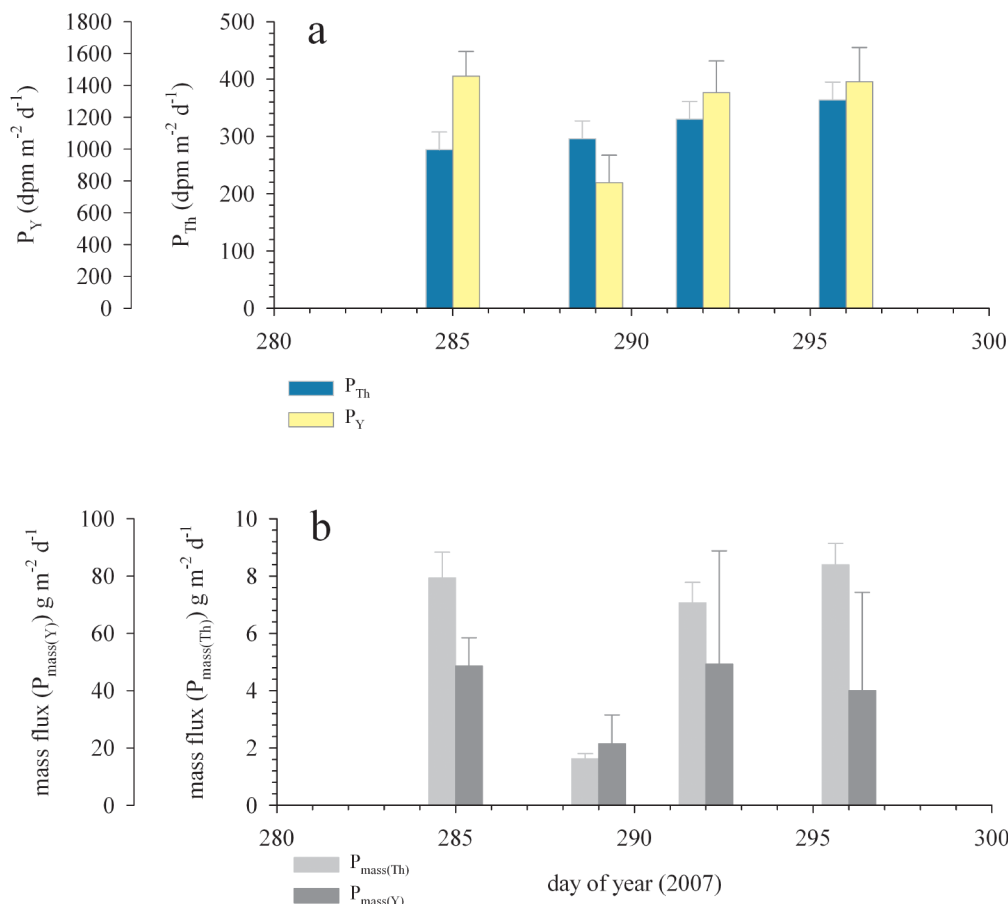


Fig. 8. (a) Non-steady-state ²³⁴Th and steady-state ⁹⁰Y fluxes. (b) Mass fluxes as measured by ²³⁴Th and ⁹⁰Y. Note difference in scale.

We propose that the differences between $P_{mass(Th)}$ and $P_{mass(Y)}$ are due to sediment resuspension. In a mass balance model that includes sediment resuspension (but still ignores horizontal advection [V] and any autochthonous production, which we will assume here is proportionally negligible), the true net mass flux (P_{mass}) is equal to the change in the total suspended matter inventory over time ($\Delta I_{mass}/\Delta t$). Moreover:

$$\Delta I_{mass} / \Delta t = P_{mass} = P_{mass}^D - P_{mass}^R \quad (17)$$

where P_{mass}^D is the true downward flux of material, P_{mass}^R is the resuspended flux of material, and all four terms are expressed in $g\ m^{-2}\ d^{-1}$. If sediment resuspended back into the water column has retained any activity of ²³⁴Th or ⁹⁰Y from its original descent through the water column, then the resuspended activity will affect the calculation of both P_{Th} and P_Y as well as $P_{mass(Th)}$ and $P_{mass(Y)}$. As material settles to the bottom, the amount of activity supported by both parents of ²³⁴Th and ⁹⁰Y (i.e., ²³⁸U and ⁹⁰Sr) becomes negligible and any activity of ²³⁴Th or ⁹⁰Y begins to decay at a rate determined by its half-life (Fig. 9a). The extent to which resuspended sediment affects P_{Th} and P_Y or $P_{mass(Th)}$ and $P_{mass(Y)}$ will, therefore, depend upon the length of time the sediment has remained on the bottom. If material is deposited and immediately resuspended, there is no decay of either radionuclide and the resuspended mass is in effect “invisible” to both tracers (Fig. 9b). At the other extreme, if the material has resided on the bottom for a long time (>160 d), then any resuspended material will have lost the ²³⁴Th and ⁹⁰Y activity that it had gained from its initial descent through the water column, and it will appear as new material to both tracers (Fig. 9d). Between these two extremes, however, some fraction of ²³⁴Th and (possibly) ⁹⁰Y is returned to the water column (Fig. 9c). Had either extreme existed in our field measurements (i.e., 0 = time on bottom > 160 d), then the estimates of P_{Th} and P_Y and $P_{mass(Th)}$ and $P_{mass(Y)}$ (in Fig. 8) should have agreed. This is not the case here. However, we can use the known rates of ²³⁴Th and ⁹⁰Y decay, and our measured values of P_{Th} , P_Y , $mass / A_{Th}^P$, $mass / A_Y^P$ and $\Delta I_{mass} / \Delta t$ to solve for both the terms in Eq. 17 (P_{mass}^D , P_{mass}^R), and the length of time between the deposition of material on the bottom and its resuspension.

We begin by assuming that, in a system with no resuspension, the true downward flux of material as determined by ²³⁴Th ($P_{mass(Th)}^D$) is equal to the true downward flux of material as determined by ⁹⁰Y ($P_{mass(Y)}^D$):

$$P_{mass(Th)}^D = P_{mass(Y)}^D \quad (18)$$

From Eqs. 14 and 15, we can express Eq. 18 as:

$$P_{Th}^D \times \frac{mass}{A_{Th}^P} = P_Y^D \times \frac{mass}{A_Y^P} \quad (19)$$

where P_{Th}^D and P_Y^D are the true downward fluxes of ²³⁴Th and ⁹⁰Y, respectively. If we allow for resuspension and substitute

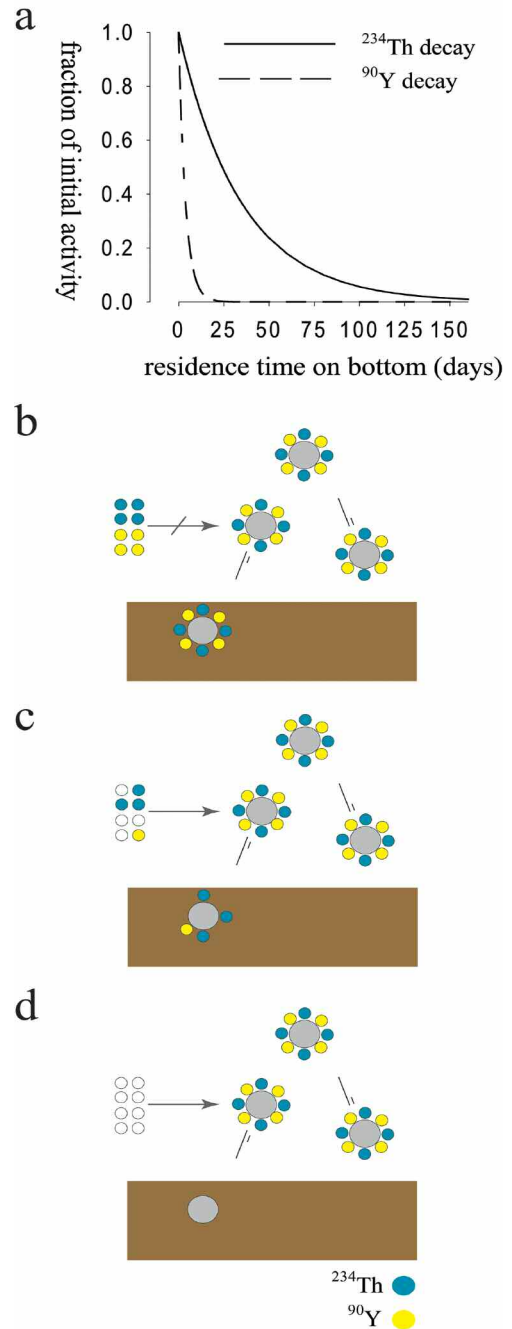


Fig. 9. (a) Activity of ²³⁴Th and ⁹⁰Y on particles as a function of residence time on the bottom. (b) Instantaneous resuspension (e.g., t_b = minutes). (c) Intermediate interval resuspension (e.g., t_b = days). (d) Long interval resuspension (e.g., t_b = months).

the true downward flux of activity with the sum of the net (P) and resuspended (P^R) activity fluxes, then Eq. 19 can be expressed as:

$$(P_{Th} + P_{Th}^R) \times \frac{mass}{A_{Th}^P} = (P_Y + P_Y^R) \times \frac{mass}{A_Y^P} \quad (20)$$

Finally, if we express the resuspended activity fluxes (P^R) as the product of the mass of resuspended material (P_{mass}^R) and the activity/mass ratios on particles ($A^P/mass$) – which are allowed to vary as a function of time spent on the bottom (t_b) – then Eq. 20 can be expressed as:

$$(P_{Th} + (P_{mass}^R \times \frac{A_{Th}^P}{mass} \times e^{-\lambda_{Th}t_b})) \times \frac{mass}{A_{Th}^P} = (P_Y + (P_{mass}^R \times \frac{A_Y^P}{mass} \times e^{-\lambda_Y t_b})) \times \frac{mass}{A_Y^P} \tag{21}$$

where we assume the water column $A^P/mass$ ratios are relatively constant over short timescales. Measured $A^P/mass$ ratios for both ²³⁴Th (excluding the second sampling event on day 289) and ⁹⁰Y varied only ~15% from each mean at 17 m depth (Table 1). From Eq. 21, we can solve for the flux of resuspended material (P_{mass}^R) as a function of how long the material resided on the bottom (t_b):

$$P_{mass}^R = - \frac{P_{Th} \times \frac{mass}{A_{Th}^P} - P_Y \times \frac{mass}{A_Y^P}}{e^{-\lambda_{Th}t_b} - e^{-\lambda_Y t_b}} \tag{22}$$

For any value of t_b , the resulting value of P_{mass}^R can be used to solve for the true downward flux of material (P_{mass}^D) using either the left or right hand side of Eq. 21; or Eq. 17 if the change in inventory of suspended material ($\Delta I_{mass}/\Delta t$) has been measured.

Material fluxes for all four cruises were calculated using measured values of P_{Th} , P_Y , $mass / A_{Th}^P$, $mass / A_Y^P$, and I_{mass} and are plotted as a function of sediment residence time (t_b) in Fig. 10. Mass balance solutions were calculated (when possible) so that net mass fluxes (P_{mass}) were equal to the observed change in the suspended matter inventory ($\Delta I_{mass}/\Delta t$) (Table 2). Estimates of uncertainty have been ignored here, but will be addressed below in a separate analysis of sensitivity. On 12 Oct (day 285), a large resuspension event resulted in an observed $\Delta I_{mass}/\Delta t$ of $-16.4 \text{ g m}^{-2} \text{ d}^{-1}$ (where negative fluxes here indicate an increase in the suspended matter inventory). Calculated values of P_{mass} intersected the observed net flux ($\Delta I_{mass}/\Delta t$) when the residence time of material on the bottom (t_b) was equal to 16.0 d. Corresponding estimates of the total downward (P_{mass}^D) and resuspended (P_{mass}^R) fluxes of material were equal to 49.7 and 66.1 $\text{g m}^{-2} \text{ d}^{-1}$, respectively. The downward flux of material as measured by ⁹⁰Y/⁹⁰Sr disequilibrium ($P_{mass(Y)}$) = 48.6 $\text{g m}^{-2} \text{ d}^{-1}$) was nearly equal to P_{mass}^D because any ⁹⁰Y that had been deposited on the bottom would have decayed after the apparent residence time of 16.0 d.

Mass fluxes on 16 Oct (day 289) were unusual. The measured inventory of suspended material (I_{mass}) dropped significantly, resulting in an observed $\Delta I_{mass}/\Delta t$ of 14.8 $\text{g m}^{-2} \text{ d}^{-1}$. Our preliminary interpretation of these results is that the conditions of our mass balance presented in Eq. 17 are invalid and (on this day at least) a term for horizontal advection (V) is required. ⁹⁰Y and ²³⁴Th inventories rose significantly on day

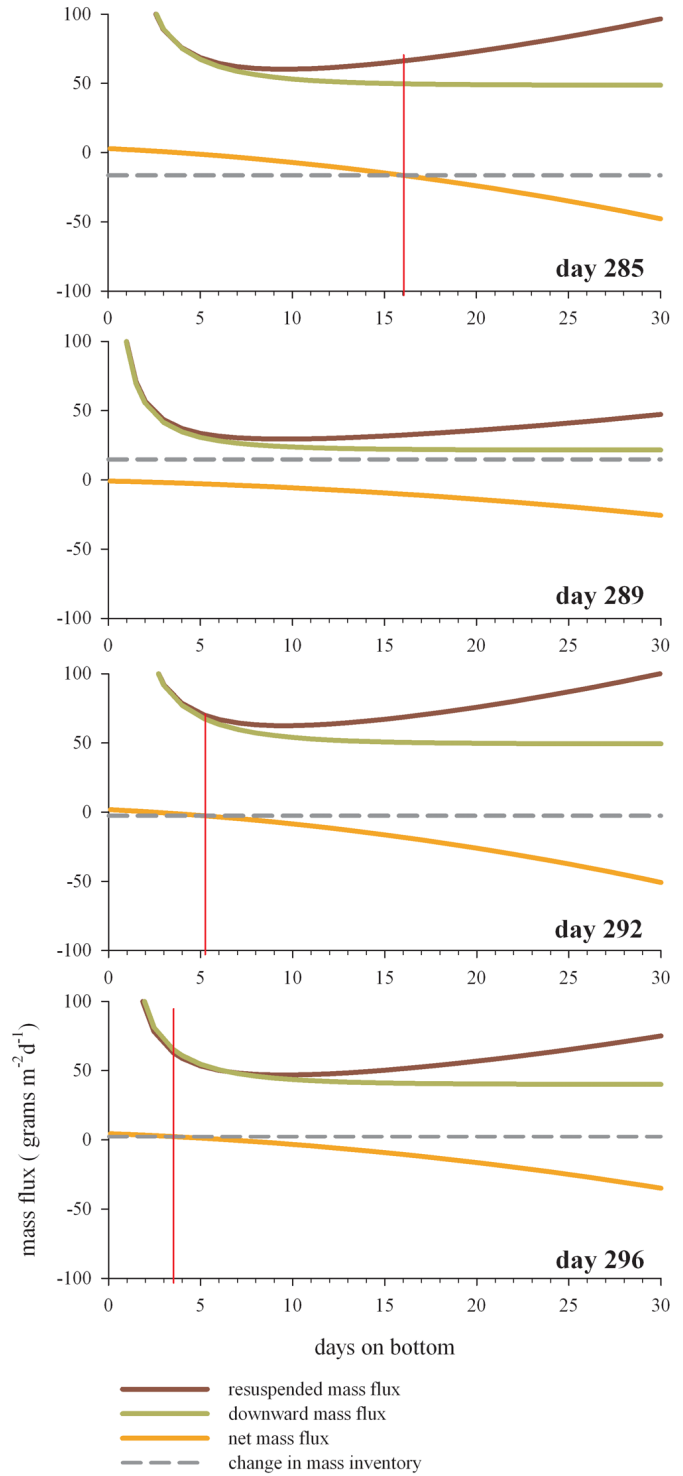


Fig. 10. Resuspended mass flux, total downward mass flux, and net mass flux as calculated by Eqs. 17, 21, and 22. Red vertical lines indicate amount of time required for sediment to reside on bottom so that calculated values of net mass flux equal observed changes in the suspended matter inventory over time.

Table 2. Fluxes of suspended material at station 'Green Can' in southern Lake Michigan (October 2007).

DOY	P_{mass}^D $\text{g m}^{-2} \text{d}^{-1}$	P_{mass}^R $\text{g m}^{-2} \text{d}^{-1}$	P_{mass} $\text{g m}^{-2} \text{d}^{-1}$	$P_{mass(Y)}$ $\text{g m}^{-2} \text{d}^{-1}$	I_{mass} g m^{-2}	ΔI_{mass} $\text{g m}^{-2} \text{d}^{-1}$	t_b d
281.5	—	—	—	—	6.8	—	—
285.5	49.7	66.1	-16.4	48.6	72.5	-16.4	16.0
289.5	—	—	—	21.5	13.4	14.8	—
292.5	67.4	70.1	-2.7	49.2	21.3	-2.7	5.2
296.5	65.4	63.0	2.4	40.0	11.9	2.4	3.5

289 (Fig. 7) and an examination of measured water currents confirms a strong influx of offshore waters from the east (Fig. 11, top panel).

On 19 Oct (day 292), the observed $\Delta I_{mass}/\Delta t$ of $-2.7 \text{ g m}^{-2} \text{d}^{-1}$ intersected the calculated values of P_{mass} after a residence time (t_b) of 5.2 d. The calculated downward flux ($P_{mass}^D = 67.4 \text{ g m}^{-2} \text{d}^{-1}$) was greater than the ^{90}Y derived mass flux ($P_{mass(Y)} = 49.2 \text{ g m}^{-2} \text{d}^{-1}$) because the shorter residence time of material on the bottom resulted in the resuspension of ^{90}Y activity (see Fig. 9). On 23 Oct (day 296), the observed ΔI_{mass} of $2.4 \text{ g m}^{-2} \text{d}^{-1}$ intersected the calculated values of P_{mass} after a residence time (t_b) of only 3.5 d, which corresponded with a P_{mass}^D estimate of $65.4 \text{ g m}^{-2} \text{d}^{-1}$. The relatively high estimates of P_{mass}^D that are made here correspond with earlier estimates of mass flux in nearshore Lake Michigan. In 2000, ^{234}Th inventories were measured in the water column and lakebed over an 8 d period. Daily estimates of deposition and resuspension ranged from $75.8 \text{ g m}^{-2} \text{d}^{-1}$ to $-90.8 \text{ g m}^{-2} \text{d}^{-1}$, respectively (Klump et al. 2003).

The range of calculated sediment residence times (t_b) can be explained by the intensity of sediment resuspension (Fig. 12). On 12 Oct (day 285), the relatively long residence time (t_b) of 16.0 d suggests the material in the water column had, on average, been residing on the bottom since \sim day 269. A large resuspension event, such as the one that began on day 284, would be expected to resuspend deeper and older material. Our continuous sonde measurement of total suspended matter only began on day 272 but showed no major resuspension event over the following 12 d interval (to day 284). On 19 Oct (day 292), the residence time (t_b) of 5.2 d suggests the suspended material last fell through the water column on day 287—which corresponds with the tail end of the large resuspension event that began on day 284. Finally, on 23 Oct (day 296), the residence time (t_b) of only 3.5 d suggests the suspended material last fell through the water column on day 293, which roughly corresponds with the tail end of the resuspension event that began on day 291.

Sensitivity analysis—The uncertainties (σ) that are associated with the flux terms that are derived here, must take into account the propagation of errors. Our discussion of error propagation here is not concerned with the results of our Oct 2007 dataset per se, but rather, the sensitivity of each radionuclide measurement to the uncertainty of our flux calculations.

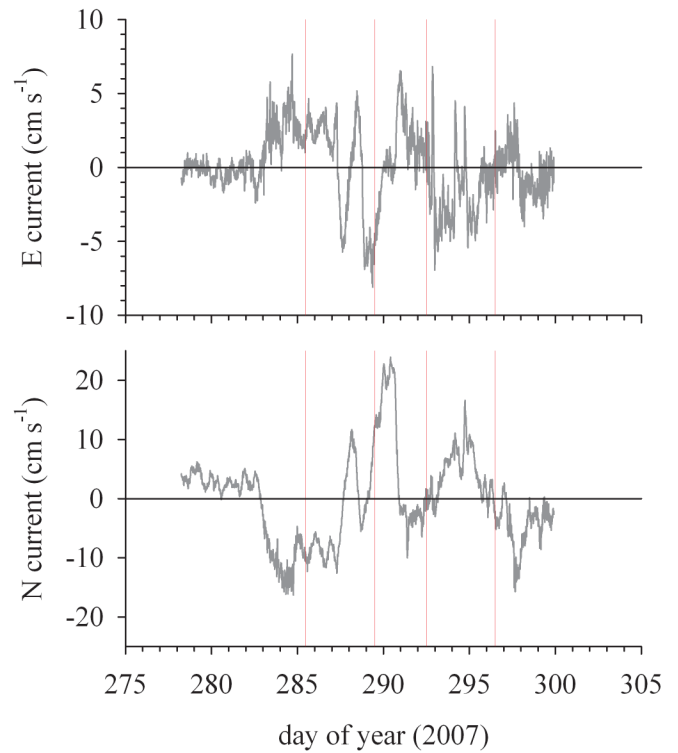


Fig. 11. Average water currents between 2 and 16 m depth at 'Green Can' station. Red vertical lines identify sampling dates on 12, 16, 19, 23 Oct 2007. (Top panel) Currents running east (off shore). (Bottom panel) Currents running north (alongshore).

If we begin with the assumption that uncertainties (σ) in $A_U, A_{Th}, A_Y, A_{Sr}, \partial A_{Th}/\partial t, mass/A_{Th}^p$, and $mass/A_Y^p$ can be made as little as $\pm 3\%$ and as great as $\pm 15\%$ in relative error ($3\% \leq \sigma_{A_U}, \sigma_{A_{Th}}, \sigma_{A_{Sr}}, \sigma_{A_Y}, \sigma_{\partial A_{Th}/\partial t}, \sigma_{mass/A_{Th}^p}, \sigma_{mass/A_Y^p} \leq 15\%$); then the overall uncertainty of P_Y (from Eq. 13) can be expressed as:

$$\sigma_{P_Y} = \lambda_Y \sqrt{\sigma_{A_{Sr}}^2 + \sigma_{A_Y}^2} \quad (23)$$

and the overall uncertainty of P_{Th} (using the non-steady-state expression of Eq. 16) can be expressed as:

$$\sigma_{P_{Th}} = \sqrt{(\lambda_{Th} \sigma_{A_U})^2 + (\lambda_{Th} \sigma_{A_{Th}})^2 + \sigma_{\partial A_{Th}/\partial t}^2} \quad (24)$$

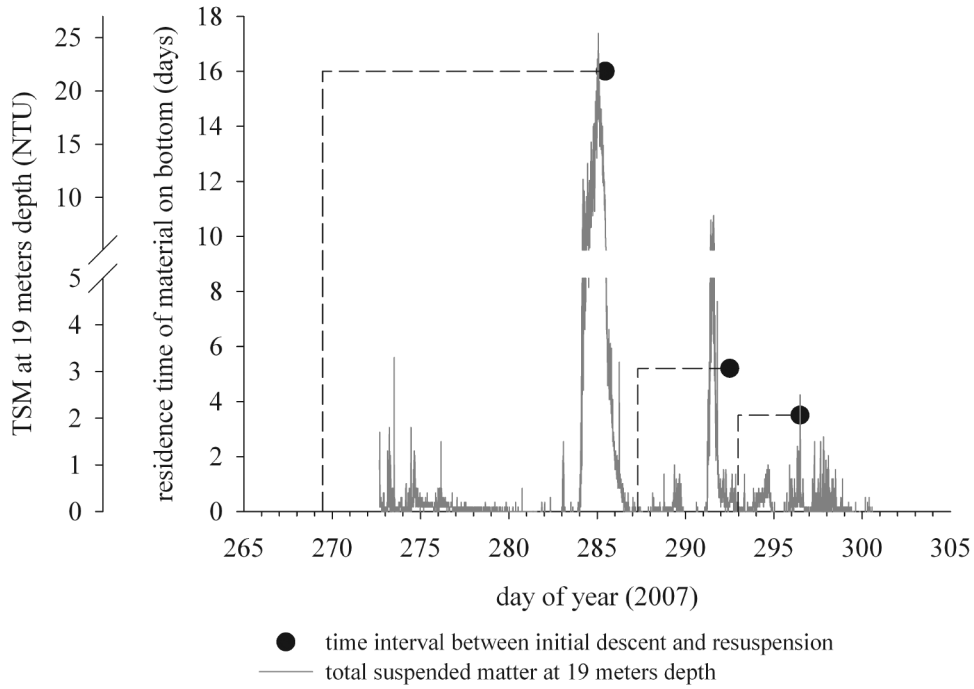


Fig. 12. Calculated ages of resuspended material in the water column on days 285, 292, and 296 are plotted against continuous sonde measurements of suspended matter at 19 m depth. Dashed lines project sediment age back to time when material last fell to the bottom.

where the uncertainties in λ_Y and λ_{Th} are assumed to be negligible. The overall uncertainties on mass fluxes derived by ²³⁴Th ($P_{mass(Th)}$) from Eq. 14 and ⁹⁰Y ($P_{mass(Y)}$) from Eq. 15 can likewise be expressed as:

$$\sigma_{P_{mass(Th)}} = P_{mass(Th)} \sqrt{\left(\frac{\sigma_{P_{Th}}}{P_{Th}}\right)^2 + \left(\frac{\sigma_{mass/A_{Th}^P}}{mass/A_{Th}^P}\right)^2} \quad (25)$$

and

$$\sigma_{P_{mass(Y)}} = P_{mass(Y)} \sqrt{\left(\frac{\sigma_{P_Y}}{P_Y}\right)^2 + \left(\frac{\sigma_{mass/A_Y^P}}{mass/A_Y^P}\right)^2} \quad (26)$$

Finally, the overall uncertainty on the flux of resuspended sediment (P_{mass}^R), from Eq. 22, can be simplified as:

$$\sigma_{P_{mass}^R} = \sqrt{\frac{\sigma_{P_{mass(Th)}}^2 + \sigma_{P_{mass(Y)}}^2}{(e^{-\lambda_{Th}t_b} - e^{-\lambda_Y t_b})^2}} \quad (27)$$

The error sensitivities of the calculated flux terms (P_{Th} , P_Y , $P_{mass(Th)}$, $P_{mass(Y)}$ and P_{mass}^R) as a function of the forced (i.e., $\pm 3\%$ and $\pm 15\%$) uncertainties of the radionuclide measurements (A_U , A_{Th} , A_Y , A_{Sr} , $\partial A_{Th}/\partial t$, $mass/A_{Th}^P$ and $mass/A_Y^P$) from 12 Oct (day 285) are presented in Fig. 13. Estimates of uncertainty associated with the flux of ²³⁴Th ($\sigma_{P_{Th}}$) ranged from a minimum of $\pm 4\%$ to a maximum of $\pm 18\%$ when all terms in Eq. 24 were given relative errors of $\pm 3\%$ and $\pm 15\%$, respectively. Relative errors of $\pm 15\%$ for either ²³⁸U or ²³⁴Th (with all other errors in Eq. 24 held to $\pm 3\%$) resulted in $\sigma_{P_{Th}}$ uncertainties of $\pm 8\%$. Estimates of P_{Th} were most sensitive to errors in $\partial A_{Th}/\partial t$.

The relative insensitivity of P_{Th} to uncertainties in either parent or daughter activity inventories relates to the large non-steady-state term of Eq. 16. Estimates of uncertainty associated with the ²³⁴Th derived mass flux ($\sigma_{P_{mass(Th)}}$) ranged from a minimum of $\pm 5\%$ to a maximum of $\pm 24\%$ when all terms in Eq. 25 were given relative errors of $\pm 3\%$ and $\pm 15\%$, respectively. Estimates of $P_{mass(Th)}$ were most sensitive to errors in $\partial A_{Th}/\partial t$ and $mass/A_{Th}^P$. Under the same conditions, estimates of uncertainty associated with the flux of ⁹⁰Y (σ_{P_Y}) and the ⁹⁰Y derived mass flux ($\sigma_{P_{mass(Y)}}$) ranged from $\pm 10\%$ to $\pm 52\%$ and $\pm 11\%$ to $\pm 54\%$, respectively. The sensitivity of σ_{P_Y} here to both A_Y and A_{Sr} in particular relates to a lack of any significant non steady-state term and the relatively high ratio of A_Y/A_{Sr} (~ 0.65). When all the errors were propagated to the calculation of the flux of resuspended sediment (P_{mass}^R), $\sigma_{P_{mass}^R}$ ranged from $\pm 13\%$ to $\pm 67\%$, with uncertainties in parent and daughter radionuclide inventories contributing the greatest source of error.

The relative importance of each radionuclide measurement in terms of its contribution to the propagated error of a flux calculation will vary with location and time and will depend strongly on the extent of disequilibrium between each daughter with its parent. We recommend, therefore, that before extensive sampling in any new aquatic system, a sensitivity analysis based on a minimum knowledge of parent activities of ²³⁸U and ⁹⁰Sr and suspended matter concentrations be carried out in advance.

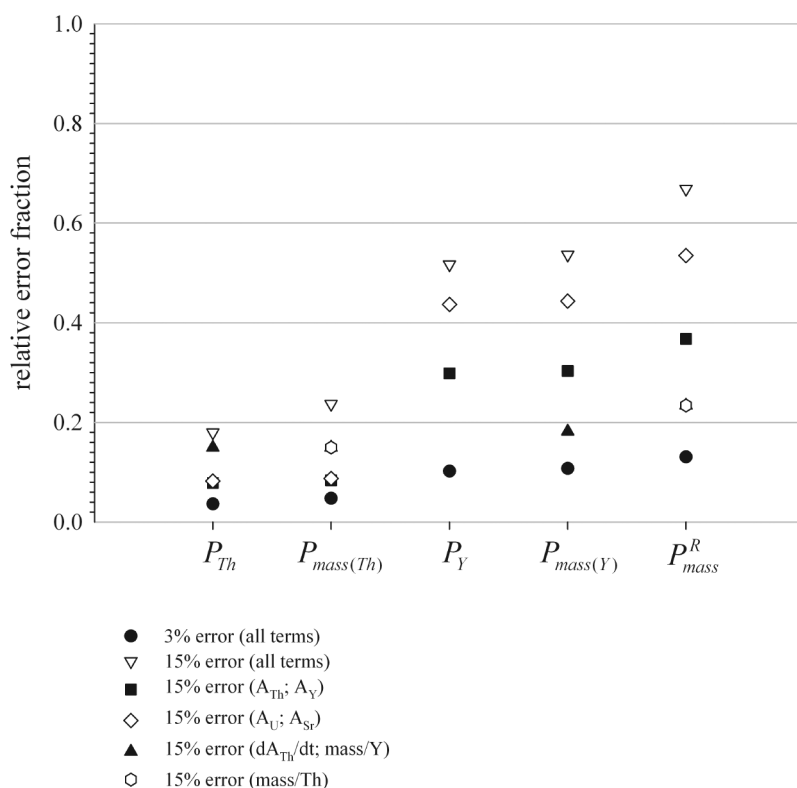


Fig. 13. Sensitivity analysis of error propagation on calculated fluxes.

Discussion

With a decay coefficient (λ) of 0.259 d^{-1} , ^{90}Y is well suited for measuring short timescale processes. With respect to ^{234}Th , ^{90}Y might offer several advantages. In an offshore environment, fluxes derived from ^{90}Y disequilibria might more closely match the timescale of particle collection in a sediment trap (Cochran et al. 2009; Buesseler et al. 2009; Lepore et al. 2009). In shallow, nearshore areas, large particle fluxes are less likely to overwhelm the rate of ^{90}Y production; and sediment resuspension events—depending on their frequency—are less likely to dampen the true estimate of gross particle removal.

When ^{90}Y and ^{234}Th disequilibrium are measured in tandem, net particle removal rates on both time scales are measured. This information can be used to calculate a variety of aquatic process rates and accelerations and ages. Here we have demonstrated how both tracers can be utilized to calculate both the flux of resuspended material to the water column and an index of the age of resuspended material. This information, in turn, might be used to better understand the formation and propagation of benthic nepheloid layers (e.g., Thomsen and van Weering 1998; Rutgers van der Loeff 2002; Hawley 2004) and their effect on nutrient cycling; or the temporal and spatial variability of planktonic and sedimentary bacteria (e.g., Neilson 1997; MacGregor et al. 2001; Mueller-Spitz et al. 2009).

In our attempt to quantify the true downward and resuspended fluxes of material in a shallow, isothermal water column, we assumed that newly produced (autochthonous) particles played an insignificant role in scavenging either ^{234}Th or ^{90}Y . This confined our modeling efforts to only one particle type. While this might be justified in other similar environments, future studies might focus on a thermally stratified offshore water column, where ^{234}Th and ^{90}Y derived flux estimates of autochthonous material from the surface layer could be incorporated into a more thorough examination of particle dynamics throughout the water column.

Comments and recommendations

Our final comments and recommendations address where and when the $^{90}\text{Y}/^{90}\text{Sr}$ tracer might be applied and possible methodological modifications.

Method application

^{90}Sr activity—We have begun to collate available publications and databases describing geographic distributions of ^{90}Sr activity in order to determine how applicable this method is to areas outside of the Laurentian Great Lakes. In freshwater systems, in the Northern Hemisphere at least, relatively high activities of ^{90}Sr (~ 0.3 to 0.9 dpm L^{-1}) appear common enough that the use of the $^{90}\text{Y}/^{90}\text{Sr}$ tracer pair for tracking and evaluating particle transport rates and reaction processes appears feasible. (See, for example, the following sources: Joshi 1991; Smith et al. 2004; European

Commission Joint Research Centre 2009; EPA RadNet 2009)

In nearshore coastal marine areas that are affected by riverine runoff, liquid discharges from European nuclear reprocessing plants (e.g., Sellafield and Cap de la Hague), or to a lesser extent, fallout from the Chernobyl accident, there appear to be areas where sufficient ^{90}Sr activity is available for use as a tracer. In the Irish Sea, for instance, average ^{90}Sr activities in the year 2000 were reported to be 3.0 dpm L^{-1} (IAEA 2005). In the North Atlantic and other open offshore marine systems, however, ^{90}Sr activities are falling below ~ 0.1 dpm L^{-1} (IAEA 2005). If $^{90}\text{Y}/^{90}\text{Sr}$ disequilibrium is to be exploited as a particle flux tracer here, then larger water samples are required.

Flux magnitude—In systems where the flux of material out of the water column is particularly low, the rapid ingrowth of ^{90}Y may result in $^{90}\text{Y}/^{90}\text{Sr}$ ratios that, statistically, are indistinguishable from secular equilibrium. The information gathered, however, could be used to provide an upper boundary on particle fluxes.

Method modification

Sampling—Our initial estimate of a 50-L water sample was, in hindsight, probably too low for the environment that we sampled in nearshore Lake Michigan. Low particle concentrations combined with a relatively low ^{90}Y particle distribution coefficient (K_d), resulted in large propagated errors on our measurements of particle-bound ^{90}Y fractions (e.g., Table 1, Fig. 8b; day 292, 296). We recommend, therefore, the particulate sampling protocol for ^{234}Th discussed in Rutgers van der Loeff et al. (2006, and references therein), where a large volume of water is filtered immediately onsite for particulate radionuclide activities and a smaller volume of water is collected for total radionuclide activities.

Yield monitors—Yield monitors (e.g., ^{229}Th and ^{88}Y) are critical for determining the recovery of ^{234}Th and ^{90}Y from the original sample matrix. As stated earlier, however, both ^{229}Th and ^{88}Y have the potential to positively bias the calculated activity of ^{90}Y if the activity of ^{90}Y is very low. We recommend, therefore, that when measured ^{90}Y activities are low, beta contributions from both yield monitors should be rigorously accounted for. Alternatively, different yield monitors could be employed. ^{230}Th , for instance, is commonly used as a yield monitor for ^{234}Th (Rutgers van der Loeff et al. 2006), and it would have no effect on ^{90}Y activity calculations. Similarly, (stable) ^{89}Y could be used as a replacement for ^{88}Y .

References

- Alberts, J. J., and M. A. Wahlgren. 1981. Concentrations of 239 , ^{240}Pu , ^{137}Cs , and ^{90}Sr in the waters of the Laurentian Great Lakes: Comparisons of 1973 and 1976 values. *Environ. Sci. Technol.* 15:94-98 [doi:10.1021/es00083a010].
- Aller, R. C., and J. K. Cochran. 1976. $^{234}\text{Th}/^{238}\text{U}$ disequilibrium in near-shore sediment: particle reworking and diagenetic timescales. *Earth Planet. Sci. Lett.* 29:37-50 [doi:10.1016/0012-821X(76)90024-8].
- Bhat, S. G., S. Krishnaswamy, D. Lal, Rama, and W. S. Moore. 1969. $^{234}\text{Th}/^{238}\text{U}$ ratios in the ocean. *Earth Planet. Sci. Lett.* 5:483-491.
- Buesseler, K. O., and others. 2001. Upper ocean export of particulate organic carbon and biogenic silica in the Southern Ocean along 170 degrees W. *Deep-Sea Res. II* 48(19-20):4275-4297 [doi:10.1016/S0967-0645(01)00089-3].
- , S. Pike, K. Mati, C. H. Lamborg, D. A. Siegel, and T. W. Trull. 2009. Thorium-234 as a tracer of spatial, temporal and vertical variability in particle flux in the North Pacific. *Deep-Sea Res. I* 56(7): 1143-1167 [doi:10.1016/j.dsr.2009.04.001].
- Cochran, J. K., and others. 2009. Time-series measurements of Th-234 in water column and sediment trap samples from the northwestern Mediterranean Sea. *Deep-Sea Res. II* 56(18):1487-1501 [doi:10.1016/j.dsr2.2008.12.034].
- Consi, T. R., T. F. Hansen, and J. V. Klump. 2007. GLUCOS: The Great Lakes Urban Coastal Observing System—A radio-linked buoy network for real-time monitoring of water quality in an urban freshwater coastal zone. *Sea Technol.* 48 (9):39-45.
- Durham, R. 1981. Canadian Centre for Inland Waters (CCIW) annual report.
- Environmental Protection Agency (EPA) RadNet database (formerly Environmental Radiation Ambient Monitoring System – ERAMS). 2009. <<http://www.epa.gov/enviro/html/erams/adhoc.html>; accessed 15 December 2009>.
- European Commission Joint Research Centre. 2009. Radioactivity Environmental Monitoring Program (REM), Environmental radioactivity in the European Community 2004-2006. <<http://rem.jrc.ec.europa.eu/RemWeb/Reports.aspx>>.
- Friedlander, G., J. W. Kennedy, and J. M. Miller. 1964. Nuclear and radiochemistry, 2nd ed. Wiley.
- Golchert, N. W., and R. G. Kolzow. 1999. Argonne National Laboratory (Environment, Safety and Health Division)—East Site Environmental Report for Calendar Year 1998. ANL Report ANL-99/3.
- Gustafson, P. F. 1984. Argonne National Laboratory, Environmental Research Division Annual Report. ANL Report ANL-83-100 (Part III).
- Hawley, N. 2004. Response of the benthic nepheloid layer to near-inertial internal waves in southern Lake Michigan. *J. Geophys. Res. Oceans.* 109:ARTN C04007 2004 [doi:10.1029/2003JC002128].
- International Atomic Energy Agency (IAEA). 2005. Worldwide marine radioactivity studies (WOMARS)—Radionuclide levels in oceans and seas. IAEA Report IAEA-TECDOC-1429. <http://www-pub.iaea.org/MTCD/publications/PDF/TE_1429_web.pdf>.
- Joshi, S. R. 1991. Radioactivity in the Great-Lakes. *Sci. Total Environ.* 100:61-104 [doi:10.1016/0048-9697(91)90374-N].
- Klump, J. V., D. N. Edgington, J. T. Waples, D.C. Szmania, B. E. Brown, and K. A. Orlandini. 2003. Sampling methods and approaches using radionuclide tracers in the study of sediment resuspension and cross margin transport in the

- nearshore of the Laurentian Great Lakes. *Int. J. Sed. Res.* 18(2):266-277.
- Lepore, K., and others. 2009. Sediment trap-and-pump-size-fractionated POC/ ^{234}Th ratios in the Mediterranean Sea and Northwest Atlantic: Implications for POC export. *Deep-Sea Res. I* 56(4): 599-613 [doi:10.1016/j.dsr.2008.11.004].
- MacGregor, B. J., D. P. Moser, B. J. Baker, E. W. Alm, M. Maurer, K. H. Nealson, and D. A. Stahl. 2001. Seasonal and spatial variability in Lake Michigan sediment small-subunit rRNA concentrations. *Appl. Environ. Microbiol.* 67(9): 3908-3922 [doi:10.1128/AEM.67.9.3908-3922.2001].
- Mueller-Spitz, S. R., G. W. Goetz, and S. L. McLellan. 2009. Temporal and spatial variability in nearshore bacterioplankton communities of Lake Michigan. *FEMS Microbiol. Ecol.* 67(3):511-522 [doi:10.1111/j.1574-6941.2008.00639.x].
- Nealson, K. H. 1997. Sediment bacteria: Who's there, what are they doing, and what's new? *Ann. Rev. Earth Planet. Sci.* 25:403-434 [doi:10.1146/annurev.earth.25.1.403].
- Orlandini, K. A., J. W. Bowling, J. E. Pinder, and W. R. Penrose. 2003. ^{90}Y - ^{90}Sr disequilibrium in surface waters: Investigating short-term particle dynamics by using a novel isotope pair. *Earth Planet. Sci. Lett.* 207:141-150 [doi:10.1016/S0012-821X(02)01096-8].
- Rutgers van der Loeff, M., and others. 2006. An overview of present techniques and methodological advances in analyzing ^{234}Th in aquatic systems. *Mar. Chem.* 100 (3-4):190-212 [doi:10.1016/j.marchem.2005.10.012].
- Rutgers van der Loeff, M. M., R. Meyer, B. Rudels, and E. Racher. 2002. Resuspension and particle transport in the benthic nepheloid layer in and near Fram Strait in relation to faunal abundances and Th-234 depletion. *Deep-Sea Res. I* 49(11):1941-1958 [doi:10.1016/S0967-0637(02)00113-9].
- Saito, N. 1984. Selected data on ion exchange separations in radioanalytical chemistry. *Pure Appl. Chem.* 56(4):523-539 [doi:10.1351/pac198456040523].
- Savoie, N. A., and others. 2006. ^{234}Th sorption and export models in the water column: A review. *Mar. Chem.* 100:234-249 [doi:10.1016/j.marchem.2005.10.014].
- Smith, J. T., and others. 2004. Global analysis of the riverine transport of Sr-90 and Cs-137. *Environ. Sci. Technol.* 38(3): 850-857 [doi:10.1021/es0300463].
- Thomsen, L., and T. C. E. van Weering. 1998. Spatial and temporal variability of particulate matter in the benthic boundary layer at the NW European Continental Margin (Goban Spur). *Progr. Oceanogr.* 42:61-76 [doi:10.1016/S0079-6611(98)00028-7].
- Wahlgren, M. A., and D. M. Nelson. 1975. Plutonium in the Laurentian Great Lakes: comparison of surface waters. *Verh. Internat. Verein. Limnol.* 19:317-322.
- Waples, J. T., K. A. Orlandini, K. M. Weckerly, D. N. Edgington, and J. V. Klump. 2003. Measuring low concentrations of Th-234 in water and sediment. *Mar. Chem.* 80(4):265-281 [doi:10.1016/S0304-4203(02)00118-4].
- , ———, D. N. Edgington, and J. V. Klump. 2004. Seasonal and spatial dynamics of $^{234}\text{Th}/^{238}\text{U}$ disequilibria in southern Lake Michigan. *J. Geophys. Res.* 109:C10S06 [doi:10.1029/2003JC002204].

Submitted 17 December 2009

Revised 17 September 2010

Accepted 8 October 2010